Available online at www.sciencedirect.com
ScienceDirect
Nuclear Physics A 814 (2008) 144–158
NUCLEAR PHYSICS A
www.elsevier.com/locate/nuclphysa

# The $^3$He$(\alpha, \gamma)^7$Be S-factor at solar energies: The prompt $\gamma$ experiment at LUNA

H. Costantini [a,*,1], D. Bemmerer [b], F. Confortola [a], A. Formicola [c], Gy. Gyürky [d], P. Bezzon [e], R. Bonetti [f,✠], C. Broggini [g], P. Corvisiero [a], Z. Elekes [d], Zs. Fülöp [d], G. Gervino [h], A. Guglielmetti [f], C. Gustavino [c], G. Imbriani [i], M. Junker [c], M. Laubenstein [c], A. Lemut [a], B. Limata [i], V. Lozza [g], M. Marta [f], R. Menegazzo [g], P. Prati [a], V. Roca [i], C. Rolfs [j], C. Rossi Alvarez [g], E. Somorjai [d], O. Straniero [k], F. Strieder [j], F. Terrasi [l], H.P. Trautvetter [j]

[a] *INFN and Dipartimento di Fisica, Università di Genova, Genova, Italy*
[b] *Forschungszentrum Dresden-Rossendorf, Dresden, Germany*
[c] *INFN, Laboratori Nazionali del Gran Sasso, L'Aquila, Italy*
[d] *ATOMKI, Debrecen, Hungary*
[e] *INFN, Laboratori Nazionali di Legnaro, Padova, Italy*
[f] *Istituto di Fisica Generale Applicata, Università di Milano & INFN Milano, Milano, Italy*
[g] *INFN Padova, Italy*
[h] *Dipartimento di Fisica Sperimentale, Università di Torino & INFN Torino, Torino, Italy*
[i] *Dipartimento di Scienze Fisiche, Università "Federico II" & INFN Napoli, Napoli, Italy*
[j] *Institut für Experimentalphysik III, Ruhr-Universität Bochum, Bochum, Germany*
[k] *INAF, Osservatorio Astronomico di Collurania, Teramo, Italy*
[l] *Dipartimento di Scienze Ambientali, Seconda Università di Napoli, Caserta & INFN Napoli, Napoli, Italy*

Received 11 July 2008; received in revised form 2 September 2008; accepted 23 September 2008

Available online 1 October 2008

**Abstract**

The $^3$He$(\alpha, \gamma)^7$Be process is a key reaction in both Big-Bang nucleosynthesis and p–p chain of Hydrogen Burning in Stars. A new measurement of the $^3$He$(\alpha, \gamma)^7$Be cross section has been performed at the

* Corresponding author. Tel.: +39 010 353 6336; fax: +39 010 314218.
*E-mail address:* costant@ge.infn.it (H. Costantini).
[1] Dipartimento di Fisica, Via Dodecaneso 33, 16146 Genova, Italy.
✠ Deceased.


doi:10.1016/j.nuclphysa.2008.09.014

INFN Gran Sasso underground laboratory by both the activation and the prompt $\gamma$ detection methods. The present work reports full details of the prompt $\gamma$ detection experiment, focusing on the determination of the systematic uncertainty. The final data, including activation measurements at LUNA, are compared with the results of the last generation experiments and two different theoretical models are used to obtain the $S$-factor at solar energies.


*PACS:* 25.55.-e; 26.20.+f; 26.35.+c; 26.65.+t

*Keywords:* NUCLEAR REACTIONS $^3$He$(\alpha, \gamma)^7$Be, $E = 220$, 250, 400 keV; measured $E_\gamma$, $I_\gamma$, $\sigma$, branching ratio; deduced astrophysical S-factor. Prompt $\gamma$ texhnique, HPGe detector in the Gran Sasso undreground laboratory. Comparison with other data

## 1. Introduction

The $^3$He$(\alpha, \gamma)^7$Be reaction is the onset of the $^7$Be and $^8$B branches of the pp-chain in hydrogen burning from which the $^7$Be and $^8$B neutrinos are generated. Thanks to the recent precise measurements performed by SNO and SuperKamiokande [1,2], the $^8$B neutrino flux is known with a 3.5% of uncertainty, while the $^7$Be neutrino flux will be measured by Borexino and Kamland in a near future with similar precision [3,4]. The solar neutrino flux depends on both astrophysical inputs, such as the luminosity, the radiative opacity, the diffusion and the elemental composition, and on nuclear physics inputs, i.e. the rates of nuclear reactions involved in the pp-chain. The uncertainty on the input parameters directly translates into uncertainties in the neutrino flux prediction. To obtain information on the astrophysical parameters from the solar neutrino flux, it is therefore necessary to know the nuclear reaction rates with an uncertainty similar to that of the measured neutrino flux.

Furthermore the $^3$He$(\alpha, \gamma)^7$Be is a fundamental reaction in Big-Bang Nucleosynthesis (BBN), since, according to the Standard Model of BBN, $^7$Li is produced almost exclusively by the $^3$He$(\alpha, \gamma)^7$Be reaction followed by the decay of $^7$Be. The large discrepancy of more than a factor two between the predicted and the observed $^7$Li abundance [5] is up to now, not understood. While it is unlikely that the explanation could come from a better knowledge of the $^3$He$(\alpha, \gamma)^7$Be reaction rate, the latter represents the necessary basis of the search for possible different solutions to the $^7$Li problem.

The $^3$He$(\alpha, \gamma)^7$Be reaction is a capture process that occurs through the formation of a $^7$Be nucleus with the emission of $\gamma$-radiation coming from the direct capture into the ground state and into the first excited state of $^7$Be. The $^7$Be decays by EC to the first excited state of $^7$Li with a branching ratio of $10.44 \pm 0.04\%$ [6] and subsequently emits a $\gamma$ of 478 keV. In the last forty years, the reaction has been studied either detecting the prompt $\gamma$ rays or detecting the delayed $\gamma$ from the decay of $^7$Be. The overall analysis presented in [7] quotes an uncertainty on the $^3$He$(\alpha, \gamma)^7$Be reaction rate coming from the discrepancy between the results obtained by measuring the reaction using the above two methods. This uncertainty (9%) has been the highest among the nuclear physics inputs adopted in the SSM [8].

In the last four years a new series of measurements has begun, starting with an activation measurement [9]. These new studies tried to measure the reaction with high precision and therefore to investigate the possible discrepancy between the two techniques that could be given either to some underestimated systematic errors or to some possible non-radiative transitions [10,11]. The aim of our experiment was therefore to provide high precision data obtained simultaneously

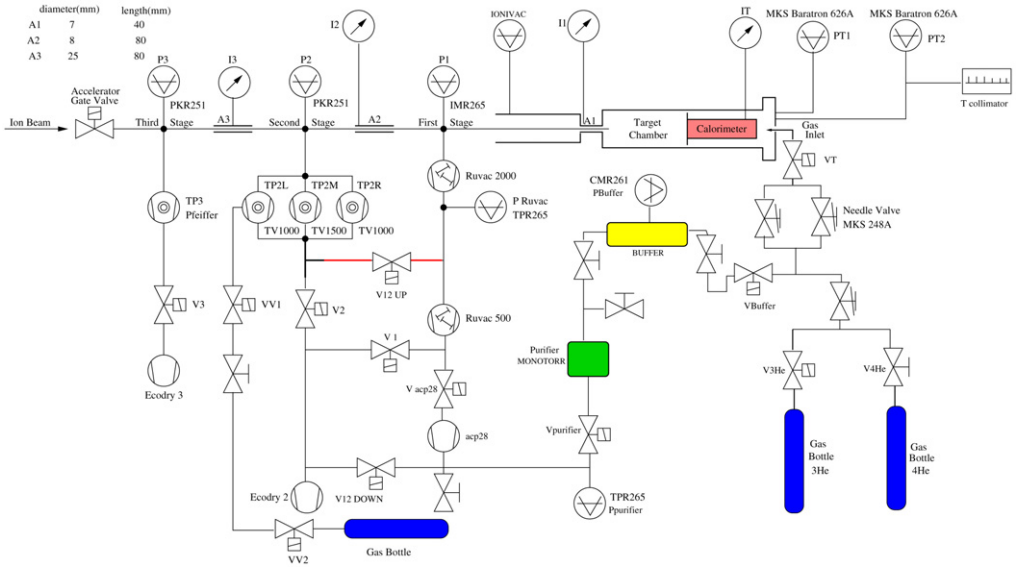


Fig. 1. Schematic drawing of the setup with windowless gas target including the three pumping stages, the interaction chamber and the $^3$He recirculation and purification system [18].

using both methods. Here we present with full details the prompt $\gamma$ approach focusing on the analysis of systematic errors.

## 2. The experimental setup

The simultaneous measurement of the prompt and the delayed $\gamma$ of the $^3$He$(\alpha,\gamma)^7$Be reaction, was carried out at the Laboratory for Underground Nuclear Astrophysics (LUNA) situated deep underground at the Gran Sasso INFN Laboratory (LNGS). The unique cosmic background suppression offered by 3800 meters water equivalent rocks of the Gran Sasso mountain, has given the possibility in the last two decades to measure several nuclear reactions belonging to the pp chain and CNO cycle of Hydrogen burning in stars [12–15].

The $^3$He$(\alpha,\gamma)^7$Be reaction cross section was studied at energies $E_\alpha = 220$, 250 and 400 keV using the 400 kV LUNA2 accelerator which delivers an $\alpha$ beam of approximately 250 μA with an uncertainty on the energy calibration of 300 eV [16]. The measurement was performed using an extended windowless $^3$He gas target setup. The gas target system has already been described elsewhere [17]. Briefly, it consists in a series of differential pumping stages separated by high flow impedance collimators (A1, A2 and A3 in Fig. 1) that allow the pressure to drop from a typical value of 0.7 mbar in the target chamber to $10^{-6}$ mbar, that is the pressure of the accelerator tube. During the experiment the $^3$He gas was recovered from the first and the second pumping stages, purified through an industrial purifier (Saes Getter MonoTorr II), and fed back to the target chamber (see Fig. 1). The pressure inside the target chamber was continuously monitored during the experiment with capacitance gauges at two different positions (PT1 and PT2 in Fig. 1): one close to the entrance collimator, and an other approximately at the center of the target chamber. The pressure and temperature profile inside the target chamber and in the connecting pipe between the interaction chamber and the first pumping stage have been measured with a dedicated chamber identical to the one used during the measurements, but with several apertures along the

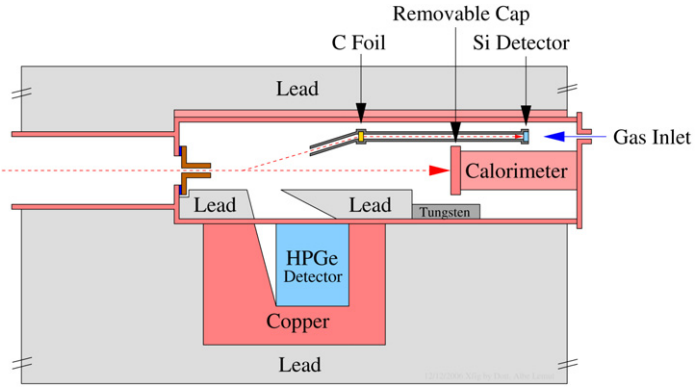


Fig. 2. Schematic view of the interaction chamber with the position of the HPGe detector and of the 100 μm silicon detector used for $^{3}$He density monitoring. The distance between the entrance collimator and the calorimeter is 35 cm.

target length. From these measurements the target thickness without beam was obtained with an uncertainty of 0.8% [17]. Due to the intense $\alpha$ beam, the target density along the beam path was decreasing due to the well-known beam heating effect [19]. This phenomenon was investigated using a 100 μm thick silicon detector positioned inside the target chamber, detecting the projectiles elastically scattered first in the target gas and subsequently in a movable 15 μg/cm$^2$ carbon foil. This effect was measured at different target gas pressures and at different positions in the target along the beam path. Details on the elastic scattering measurements are described elsewhere [20]. The purity of the target was also monitored using the elastic scattering [20] and during the whole experiment the nitrogen contamination always remained below 2.7%. The overall uncertainty on the target density considering the without-, the with-beam density measurements and the uncertainty on the gas purity corrections, is of 1.5%.

The beam entered the interaction chamber through a 7 mm diameter collimator and was stopped on a detachable copper disk that served as the primary catcher for the produced $^{7}$Be and as the hot side of a calorimeter (see Fig. 2). The latter was used to measure the beam intensity from the difference between the calorimeter power values with and without beam and was similar to the one previously used [15]. The calorimeter was calibrated in the whole energy range, using the evacuated target chamber as a Faraday cup. The calibration was periodically repeated during the entire measurement. The reproducibility of the calibrations was within 1.5%: this value was adopted as the uncertainty on the beam current determination.

## 3. The background reduction

The prompt $\gamma$ rays coming from the direct capture to the first excited state and ground state of the $^{7}$Be nucleus, were detected by a 137% (relative efficiency) HPGe detector (Fig. 2) positioned with its front face 7 cm from the beam axis. Since the energies of the prompt $\gamma$ rays (0.4, 1.3 and 1.7 MeV) are in the energy region of natural radioactive isotopes, a massive 0.3 m$^3$ copper and lead shielding was built around the detector and the target chamber. Passive shielding is particularly effective underground since the muon flux, coming from cosmic rays that, at surface, produces energetic neutrons which, in turn, may give rise to $\gamma$ rays in the lead, is reduced by six orders of magnitude in the Gran Sasso laboratory. The entire shielding was enclosed in a anti-radon envelope, which is a plexiglas box flushed with $N_2$ gas to avoid $^{222}$Rn background.

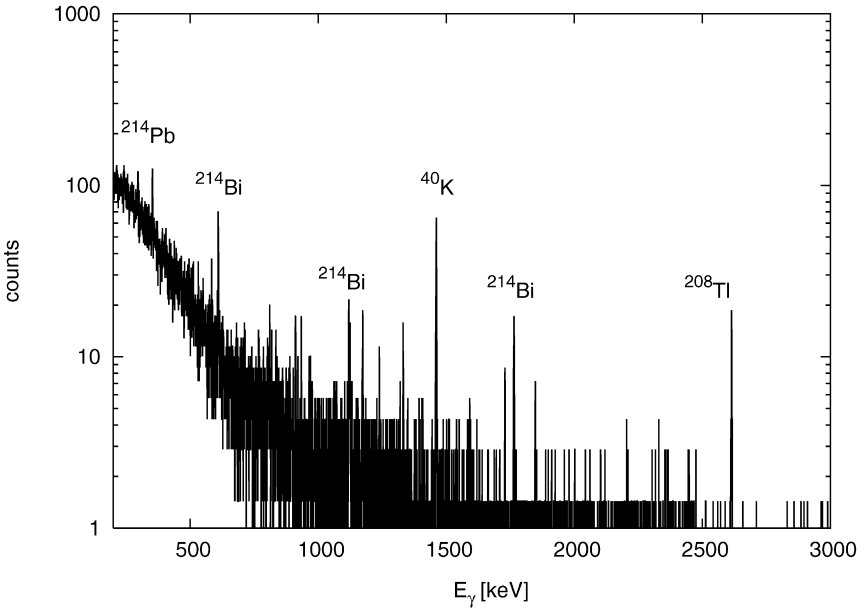


Fig. 3. Laboratory background spectrum taken with the shielded 137% HPGe detector. Measuring time was 31 days and counting rate was 0.05 counts/day/keV and 0.11 counts/day/keV in the energy region of interest for the transition to the ground and to the first excited state, respectively. At the lowest explored energy ($E_\alpha = 220$ keV) the reaction rate was 1.04 counts/day/keV and 0.57 counts/day/keV for the transition to the ground and to the first excited state, respectively.

Similar shielding was used for the off-line measurements (activation method). To further reduce the background on the detector, the target chamber was built with oxygen free high conductivity copper (OFHC) and no welding materials were used in the chamber assembly. Moreover low activity materials were used to build the silicon detector support and all the equipment inside the target chamber (Fig. 2). In this way, a background suppression of 5 orders of magnitude was reached for $\gamma$ rays below 2 MeV with respect to a background spectrum measured underground with no shielding [21]. Fig. 3 shows the background spectrum. Aside from radioactive isotopes, background could come also from beam induced reactions. A background measurement at $E_\alpha = 400$ keV substituting $^3$He gas with inert $^4$He gas was performed but no additional counts were detected with respect to the laboratory background. Further details regarding the $\gamma$ ray background can be found elsewhere [21].

## 4. Angular distribution effects and detection efficiency

According to DC model calculations [22] the $^3\mathrm{He}(\alpha,\gamma)^7\mathrm{Be}$ direct capture mainly proceeds by E1 transition that can occur through s- or d-waves. The angular distribution function $W(\theta)$ can be expressed as:

$$W(\theta) = 1 + a_1 P_1(\theta) + a_2 P_2(\theta) + \cdots, \tag{1}$$

where $a_1$ and $a_2$ are the coefficients of the Legendre polynomials $P_1(\theta)$ and $P_2(\theta)$. To minimize the systematic error due to angular distribution uncertainty, a lead collimator has been inserted inside the target chamber (Fig. 2) to collect at the HPGe detector mostly the $\gamma$ rays emitted around 55°, angle at which the second Legendre polynomial vanishes.

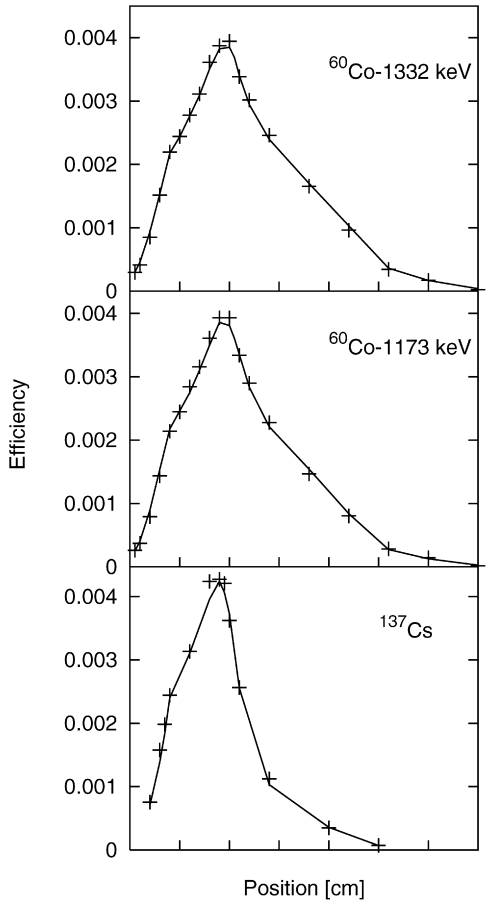


Fig. 4. Efficiency profiles measured using point-like sources of $^{60}$Co and $^{137}$Cs with the inner lead and tungsten collimators in the chamber. Crosses represent the experimental data while lines are linear interpolations of MC calculations. The zero position corresponds to the entrance of the beam inside the target chamber.

This collimator is a lead brick, 3 cm thick, with a hole shaped as a truncated cone with elliptical base and the main axis inclined with respect to the vertical of 45° (Fig. 2). This particular shape was studied with the LUNA Monte Carlo (MC) code [23] taking into account the extended target effect and the detector solid angle, which depends on the HPGe detector dimensions and its distance from the beam. The lead collimator and a tungsten brick (1.6 cm thick) were positioned in the target chamber also to shield the detector from possible beam induced radiations coming from the calorimeter cap, and from laboratory background coming from the upstream and downstream apertures in the shielding. In an extended gas target, the interactions are taking place along the whole beam path and each interaction has a different geometrical subtending angle to the detector. The detection efficiency profile $\eta(z)$ has been measured moving a $^{60}$Co ($E_\gamma = 1173$, 1332 keV) and $^{137}$Cs ($E_\gamma = 662$ keV) point-like sources along the beam axis from the collimator to the calorimeter cap. Due to the particular shape of the inner lead collimator, the efficiency profile along the target length was quite complicated and the LUNA Monte Carlo simulation code was used to evaluate the detection efficiency for the $^3$He$(\alpha, \gamma)^7$Be $\gamma$ lines. The

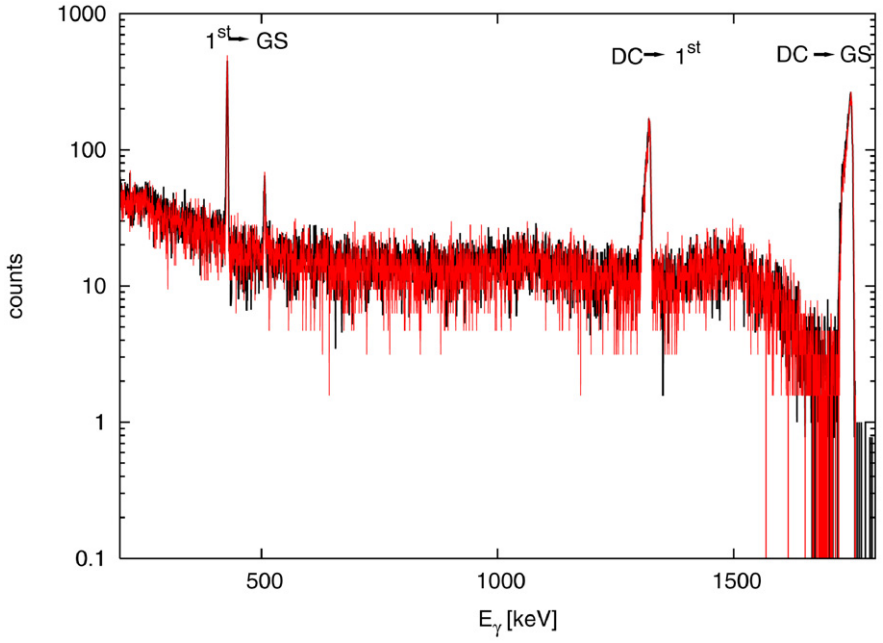


Fig. 5. Comparison between the experimental (black curve) and the simulated (red curve) $\gamma$ spectrum at $E_\alpha = 400$ keV and $P_{\text{target}} = 0.7$ mbar. The simulated spectrum was normalized to the experimental one at $E_\gamma = 1.76$ MeV to allow the shape comparison. (For interpretation of the references to colour in this figure legend, the reader is referred to the web version of this article.)

crucial point in the simulation has been the HPGe description and in particular the determination of the active volume of the detector, information not provided by the manufacturer. To determine this parameter, the inner collimator was removed from the chamber and a first set of efficiency measurements was performed using the calibrated point-like sources placed in several points along the beam path. By comparing the MC simulations with the results of these first measurements, the detector geometry was determined. Subsequently, measurements and simulations were performed with the inner lead collimator. A comparison between the simulated and the experimental efficiency profiles $\eta(z)$ is shown in Fig. 4. In the data analysis the integrated efficiency profile along the target length $L$ was used (see Eq. (3)). The percentage difference between the simulated and experimental integrated efficiency profiles is defined as:

$$\Delta_{\text{int}} = \frac{\int_0^L \eta_{\text{sim}}(z)\,dz - \int_0^L \eta_{\text{ex}}(z)\,dz}{\int_0^L \eta_{\text{ex}}(z)\,dz}, \tag{2}$$

and it turned out to be $(0.3 \pm 1.5)\%$ and $(0.6 \pm 1.5)\%$ for the 1173 and 1332 keV $\gamma$ lines of the $^{60}$Co source, respectively and $(-0.4 \pm 1.5)\%$ for the 662 keV line of the $^{137}$Cs source. The simulation reproduced the integrated experimental efficiency within the source activity uncertainties (1.5%). With the detector geometry fixed through the comparison with the $^{60}$Co and $^{137}$Cs sources, and the detailed description of the target geometry (i.e. inner Pb and W collimator geometry), the simulation reproduced the experimental $^3$He$(\alpha,\gamma)^7$Be $\gamma$ spectra at the level shown in Fig. 5. Summing effects between the primary and the secondary $\gamma$ transitions in the

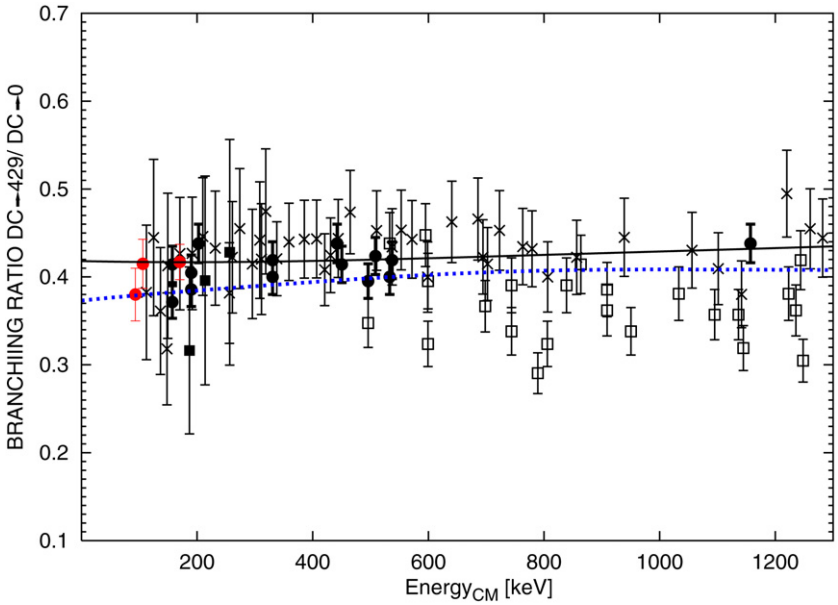


Fig. 6. Branching ratios for the $^3$He$(\alpha,\gamma)^7$Be reaction. The present data (red dots) are compared to previous experimental results from Parker and Kavanagh [26] (open squares), Nagatani et al. [27] (filled squares), Kräwinkel et al. [24] (crosses) and Osborne et al. [28] (black dotes). The solid and dotted curves are from the calculations of Liu et al. [29] and of Kajino et al. [30] respectively. (For interpretation of the references to colour in this figure legend, the reader is referred to the web version of this article.)

DC $\rightarrow$ 429 $\rightarrow$ 0 cascade, actually smaller than 1%, were considered in the MC simulation and included in the data analysis.

Angular distribution functions have previously been calculated down to 210 keV [22] and showed a small anisotropy for both the transition to the first excited state ($\gamma_1$) and to the ground state ($\gamma_0$). Experimental measurements carried out down to $E_{\rm cm} = 148$ keV [24] confirmed the anisotropy manifesting interference effects of both partial wave contributions. Recent theoretical predictions [25] are in agreement with the theoretical angular distribution functions of [22]. Predictions of $a_1$ and $a_2$ can be found in [22] as a function of the incident beam energy. These curves have been linearly extrapolated down to 200 keV and the coefficients of the Legendre polynomials adopted in the detection efficiency calculation are $a_1 = -0.05$ and $a_1 = 0$ for the transition to the ground and to the first excited state, respectively, and $a_2 = -0.1$ for both transitions. To estimate the effect on the detection efficiency of the uncertainty on the angular distribution, we have varied both $a_1$ and $a_2$ coefficients in the Monte Carlo simulation and 100% changes resulted in a global 2.5% variation of the detection efficiency. The latter has been assumed as a systematic uncertainty and turned out to be the major contribution to the error budget of the prompt $\gamma$ experiment.

The branching ratios between the two transitions $\sigma(\mathrm{DC} \rightarrow 429)/\sigma(\mathrm{DC} \rightarrow 0)$ have been measured at $E_\alpha = 400$, 250 and 220 keV and are $0.417 \pm 0.020$, $0.415 \pm 0.029$ and $0.38 \pm 0.03$, respectively. In Fig. 6 the present data are compared to previous experimental results [24,26–28] and theoretical calculations [29,30]. Although our data improve the experimental precision at low energy, they are still compatible with both theoretical predictions.

## 5. Data analysis of the prompt $\gamma$ experiment

For an extended gas target, the number of detected photons $N_\gamma$ is given by:

$$N_\gamma = N_p \int_0^L \sigma\big(E(z)\big)\eta(z)\rho_{\text{beam}}(z)\,dz, \tag{3}$$

where $N_p$ is the number of the accelerated $\alpha$-particles obtained from the calorimeter beam power measurement, $\rho_{\text{beam}}$ is the effective target density that takes into account the measured pressure, temperature profile and the beam heating effect [20], $\eta(z)$ is the detection efficiency and $\sigma$ is the reaction cross section. The length $L = 80.2$ cm is the distance between the first pumping stage and the calorimeter: according to MC simulations this region corresponds to the gas target zone where 99.9% of the detected fusion reactions take place.

Since the cross section is expected to be a smooth function at low energies [31,32], an effective cross section $\sigma_{\text{eff}}$ is introduced as the average cross section over the interaction energies:

$$\sigma_{\text{eff}} = \frac{N_\gamma}{N_p \int_0^L \eta(z)\rho_{\text{beam}}(z)\,dz}. \tag{4}$$

From the definition of the $S$-factor [33]:

$$S(E) = \frac{\sigma(E)}{E} e^{-2\pi\eta(E)} \tag{5}$$

and Eq. (4), one obtains the $S(E_{\text{eff}})$ factor, provided that an effective interaction energy $E_{\text{eff}}$ is introduced [34].

The effective energy $E_{\text{eff}}$ is defined by the relation [34]:

$$\sigma(E_{\text{eff}}) = \sigma_{\text{eff}}. \tag{6}$$

By inverting Eq. (6) one can obtain $E_{\text{eff}}$ from $\sigma^{-1}(\sigma_{\text{eff}})$. In our experimental conditions (i.e. gas pressure and beam energy), the target thickness $\Delta E$ was around 10 keV, corresponding to $6.2 \times 10^{17}$ At/cm$^2$. Therefore, since theoretical models [31,32] indicate a negligible $S(E)$ energy dependence inside $\Delta E$ at these energies, a constant $S$ factor could be considered in Eq. (5), and the effective energy was obtained from Eq. (6) that reduces to:

$$\frac{e^{-2\pi\eta(E_{\text{eff}})}}{E_{\text{eff}}} = \frac{\int_0^L \frac{e^{-2\pi\eta(E(z))}}{E(z)}\eta(z)\rho_{\text{beam}}(z)\,dz}{\int_0^L \eta(z)\rho_{\text{beam}}(z)\,dz}. \tag{7}$$

The uncertainty on the effective energy calculation is coming from the uncertainty on the beam energy (absolute calibration [16]) and from the error on the energy lost by the beam inside the target [35].

## 6. Comparison between activation and prompt results

The $^3$He$(\alpha,\gamma)^7$Be data taking lasted several months. In a first phase only activation measurements were performed: these results have been reported in [17,36]. Thereafter, a second phase (here detailed) started aimed at studying the reaction using both activation and prompt $\gamma$ method at the same time. Since the irradiation of the samples used for off-line $^7$Be counting were simultaneously performed to the $\gamma$ radiation detection, some systematic uncertainties are common to

Table 1
Systematic uncertainties and their contribution to the S-factor error for the prompt and activation experiments.

| Source | Prompt | Activation |
|---|---|---|
| Beam Intensity | 1.5% | 1.5% |
| $^3$He Target Density | 1.5% | 1.5% |
| Effective Energy | 0.5–1.1% | 0.5–1.1% |
| Angular Distribution | 2.5% | |
| Detection Efficiency | 1.5% | |
| $^7$Be counting efficiency | | 1.8% |
| Incomplete $^7$Be collection | | 0.5% |
| $^7$Be Backscattering | | 0.5% |
| $^7$Be Distribution in catcher | | 0.4% |
| 478 keV $\gamma$-ray branching | | 0.4% |
| $^7$Be Half life | | 0.1% |
| Parasitic $^7$Be production | | 0.1% |
| Total | (3.6–3.9)% | (3.0–3.2)% |

both methods and were not considered in the comparison between the $S$ factors obtained with the two techniques. In Table 1 the sources of systematic uncertainty affecting both methods and their contribution to the final uncertainty on the $S$-factor, are listed. All the LUNA results [17, 36,37] are collected in Table 2. The activation $S$-factor values obtained in the two phases of the experiment at about the same beam energy are compatible (Table 2).

## 7. Comparison with other experiments

In the last forty years the $^3$He$(\alpha,\gamma)^7$Be reaction has been extensively studied using both the activation and prompt $\gamma$ detection method. An overall analysis [7] showed an average discrepancy between $S(0)$ results obtained from the two methods of around 9%. Starting with the precise activation measurement in 2004 [9], a second generation of experiments has started with the aim of studying the $^3$He$(\alpha,\gamma)^7$Be reaction with high accuracy. Later, LUNA has measured the reaction in two different experiments: first an activation measurement with an accuracy of 3% has been reached [17,36], and subsequently the simultaneous activation and prompt measurement presented here, has been performed obtaining an average accuracy of 4%. Most recently, a new simultaneous activation and prompt measurement has been carried out [38], that extends over a larger energy range going from a minimum energy of $E_{\rm cm} = 330$ keV to a maximum energy of $E_{\rm cm} = 1230$ keV. The data were measured with an accuracy of the order of 3% [38].

In Fig. 7 the time-trend of the $S(0)$ values obtained from different experiments is shown. A clear evidence for the increase in the accuracy of the obtained $S(0)$ is visible in the second generation experiments due to a better control on the systematic effects which namely, could be the origin of the discrepancy between prompt and activation data claimed in the past [7]. Therefore we decided to consider only the data from the three most recent experiments [9,17,36–38]. Following the approach from [38] we fitted the data of the different experiments using the same theoretical curves. We used the resonating-group calculation curve of Kajino et al. [32] and the R-matrix fit of Descouvemont et al. [31]. Other theoretical trends for the S-factor are given in literature such as the one obtained with a cluster model calculation by Csoto and Langanke [43]. This approach considers non-external contributions to the cross section and therefore cannot be normalized to the experimental data.

Table 2
Summary of the LUNA prompt (p) and activation (a) data: the symbol ⋆ indicates runs in which only activation data have been collected [17,36].

| $E_{\mathrm{eff}}$ (keV) | Method | Charge (C) | Peak | Gross counts | Background counts | $\sigma(E_{\mathrm{eff}})$ (nbarn) | $S(E_{\mathrm{eff}})$ (keV b) | $\Delta S$ stat. (keV b) | $\Delta S$ syst. (keV b) |
|---|---|---|---|---|---|---|---|---|---|
| 170.1 | p | 112.7 | DC→ 0 | 6780 | 89 | $7.23 \pm 0.26$ | 0.510 | 0.008 | 0.019 |
| | p | | DC→ 429 | 3500 | 666 | $3.02 \pm 0.12$ | | | |
| 169.5 | a | 112.9 | 478→ 0 | 8666 | 579 | $10.0 \pm 0.35$ | 0.507 | 0.010 | 0.015 |
| 168.9 | a⋆ | 62.5 | 478→ 0 | 7295 | 1161 | $9.35 \pm 0.19$ | 0.482 | 0.02 | 0.03 |
| 147.7 | a⋆ | 203.1 | 478→ 0 | 10551 | 1033 | $4.61 \pm 0.07$ | 0.499 | 0.017 | 0.03 |
| 126.5 | a⋆ | 215.7 | 478→ 0 | 2866 | 95 | $1.87 \pm 0.04$ | 0.514 | 0.02 | 0.03 |
| 106.1 | p | 406.93 | DC→ 0 | 1516 | 67 | $0.415 \pm 0.018$ | 0.518 | 0.014 | 0.020 |
| | p | | DC→ 429 | 745 | 142 | $0.173 \pm 0.010$ | | | |
| 105.7 | a | 413.6 | 478→ 0 | 3764 | 1214 | $0.546 \pm 0.024$ | 0.493 | 0.015 | 0.015 |
| 93.3 | p | 636.73 | DC→ 0 | 988 | 53 | $0.171 \pm 0.008$ | 0.527 | 0.018 | 0.021 |
| | p | | DC→ 429 | 479 | 135 | $0.065 \pm 0.005$ | | | |
| 92.9 | a | 725.8 | 478→ 0 | 5123 | 2473 | $0.232 \pm 0.01$ | 0.534 | 0.016 | 0.017 |

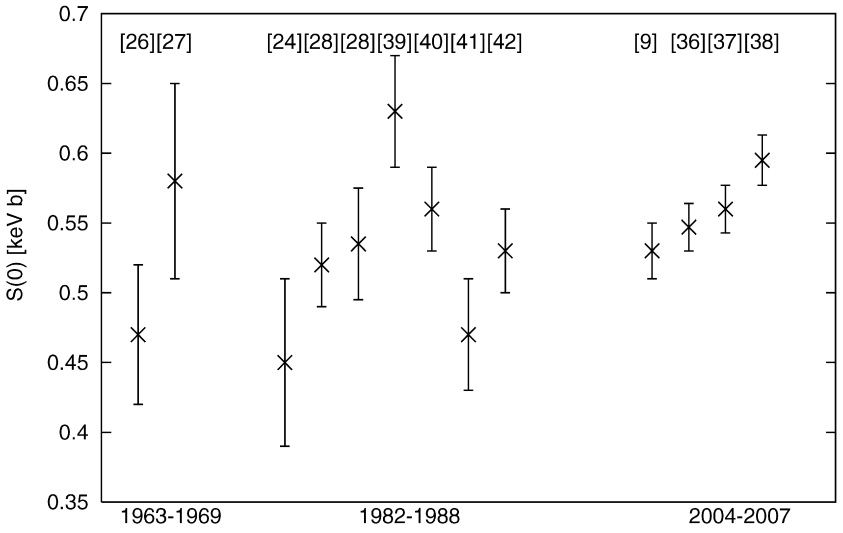


Fig. 7. $^3$He$(\alpha,\gamma)^7$Be $S(0)$ values obtained from different experiments as a function of time. Both activation and prompt $\gamma$ experiments are considered [39–42].

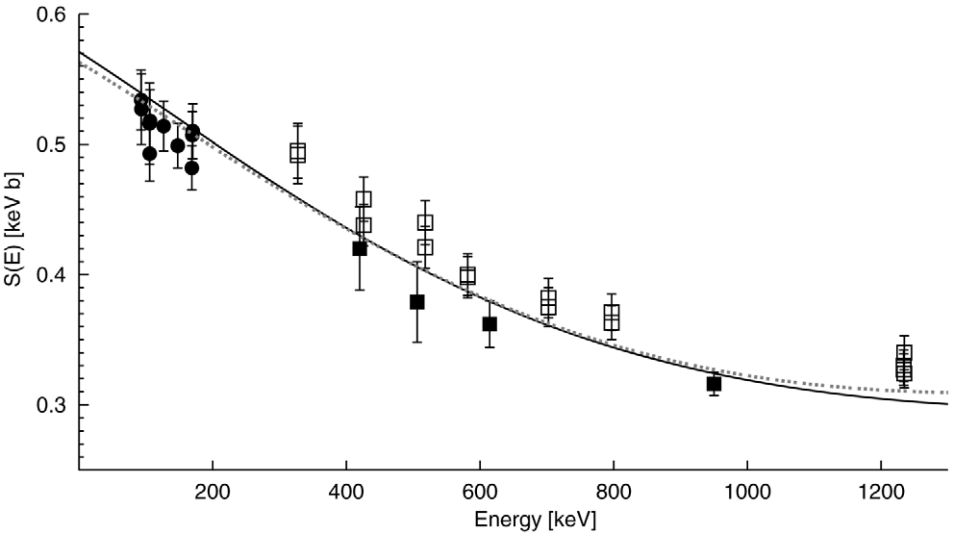


Fig. 8. Astrophysical $S$ factor for the $^3$He$(\alpha,\gamma)^7$Be reaction obtained from the most recent experiments. The filled squares are the data from Singh et al. [9], the filled circles are all the data from the LUNA experiment [17,36,37] and the open squares are all the data from Brown et al. [38]. The solid and the dotted curves are the theoretical curves by [31] and [32] respectively, obtained considering the weighted average of $S(0)$ of the different experiments as explained in the text and shown in Table 3.

The two theoretical curves [31,32] were re-scaled to the data of the different experiments and the obtained $S(0)$ values are presented in Table 3. $S(0)_A$ value is obtained from a weighted average of the $S(0)$ values from the activation measurements [9,17,36–38] while $S(0)_P$ is the weighted average of the $S(0)$ values from the prompt measurements [37,38]. The average dis-

Table 3
$S(0)$ values obtained rescaling the Kajino et al. [32] and the Descouvemont et al. [31] theoretical curves. $S(0)_A$ value is obtained from a weighted average of the $S(0)$ values from the activation measurements [9,17,36–38] while $S(0)_P$ is the weighted average of the $S(0)$ values from the prompt measurements [37,38].

| | $S(0)$ keV barn Kajino et al. [32] | $S(0)$ keV barn Descouvemont et al. [31] |
|---|---|---|
| LUNA activation data [17,36,37] | $0.548 \pm 0.017$ | $0.550 \pm 0.017$ |
| LUNA prompt data [37] | $0.561 \pm 0.021$ | $0.564 \pm 0.021$ |
| Singh et al. activation data [9] | $0.541 \pm 0.02$ | $0.551 \pm 0.02$ |
| Brown et al. activation data [38] | $0.595 \pm 0.018$ | $0.609 \pm 0.019$ |
| Brown et al. prompt data [38] | $0.596 \pm 0.021$ | $0.610 \pm 0.022$ |
| $S(0)_P$ | $0.579 \pm 0.018$ | $0.586 \pm 0.023$ |
| $S(0)_A$ | $0.562 \pm 0.017$ | $0.569 \pm 0.019$ |
| $S(0)$-TOT | $0.563 \pm 0.016$ | $0.571 \pm 0.019$ |

crepancy between prompt and activation results $\Delta S(0) = (S(0)_A - S(0)_P)/((S(0)_A + S(0)_P)/2)$ is $\Delta S(0) = -0.030 \pm 0.04$ considering the Kajino et al. theoretical curve and is $\Delta S(0) = -0.029 \pm 0.05$ considering the Descouvemont et al. R-matrix fit. This global result confirms that no discrepancy is actually observable between results obtained from the two techniques and excludes significant non-radiative contributions to the reaction cross section. Finally, we obtain a total $S(0) = 0.563 \pm 0.016$ keV b and $S(0) = 0.571 \pm 0.019$ keV b adopting the curves from [32] and from [31] respectively (see Table 3 and Fig. 8). These values are obtained from a weighted average of the $S(0)$ value of [9], of the $S(0)$ value of LUNA (activation and prompt results combined [17,36,37]) and from the $S(0)$ value of [38] (activation and prompt results combined). The final errors on $S(0)_P$, $S(0)_A$ and $S(0)$-TOT are larger than the errors obtained from a simple weighted average. Since the scatter of the points about the mean is larger than expected based on the quoted errors, we have followed the method described in [31,32,44] consisting in increasing the uncertainties on the single data so as to make the value of $\chi^2$ per degree of freedom equal to 1.0.

## 8. Conclusions

From an overall analysis of the results of the last generation experiments on $^3$He$(\alpha, \gamma)^7$Be, no discrepancy emerged between prompt and activation data. Furthermore, a total (statistical and systematical) accuracy of about 3% for the $S(0)$ value was obtained: $S(0) = 0.567 \pm 0.018 \pm 0.004$ keV b where the last term sizes the indetermination on the theoretical model adopted for the extrapolation to zero energy. However, preliminary results recently obtained with the recoil separator technique between 1 and 3 MeV [45], show a different $S$-factor energy dependence. Therefore, further improvements could come from new experiments exploring, with the same setup, the entire energy range from 0.1 to few MeV.

The present result lowers significantly the uncertainty coming from the $^3$He$(\alpha, \gamma)^7$Be nuclear reaction on the $^8$B and $^7$Be neutrino flux. As described in a recent paper by Haxton and Serenelli [46] the solar interior metallicity can be obtained by measuring the solar CN neutrino flux. The latter can be related to the measured and predicted $^8$B neutrino flux, the predicted CN neutrino flux and the C and N abundances in the solar interior (Eqs. (9) and (13) in [46]). In the near future it should be possible to measure the CN neutrino flux with experiments as Borexino [3] and the upgraded SNO experiment [47]. Thanks to the low uncertainties now achieved on the measured

rate of the key reactions $^3$He$(\alpha, \gamma)^7$Be and $^{14}$N$(p, \gamma)^{15}$O and on the precise measurement of the $^8$B neutrino flux, Borexino and SNO could determine the C and N abundances in the radiative solar core. A comparison of the Sun's deep interior and surface composition could be done, testing a key assumption of the standard solar model: a homogeneous zero-age Sun. It would also provide a cross-check on recent photospheric abundance determinations that have altered the once excellent agreement between the SSM and helioseismology [48].

## Acknowledgements

This work was supported by INFN and in part by the European Union (TARI RII3-CT-2004-506222) and OTKA (K68801 and T49245), by ILIAS integrating activity (Contract No. RII3-CT-2004-506222) as part of the EU FP6 programme and BMBF (05Cl1PC1-1).

## References

[1] B. Harmin, et al., Phys. Rev. C 72 (2005) 055502.
[2] J. Hosaka, et al., Phys. Rev. D 73 (2006) 112001.
[3] C. Arpesella, et al., Phys. Lett. B 658 (2008) 101.
[4] T. Araki, et al., Phys. Rev. Lett. 94 (2005) 081801.
[5] D. Spergel, et al., Astrophys. J. Suppl. 170 (2007) 377.
[6] D.R. Tilley, et al., Nucl. Phys. A 708 (2002) 3.
[7] E. Adelberger, et al., Rev. Mod. Phys. 70 (1998) 055502.
[8] J.N. Bahcall, M.H. Pinsonneault, Phys. Rev. Lett. 92 (2004) 121301.
[9] B.N. Singh, et al., Phys. Rev. Lett. 93 (2004) 262503.
[10] M. Nessin, T.H. Kruse, K.E. Eklund, Phys. Rev. 125 (1962) 639.
[11] K.A. Snover, A.E. Hurd, Phys. Rev. C 67 (2003) 55801.
[12] R. Bonetti, et al., Phys. Rev. Lett. 82 (1999) 5205.
[13] C. Casella, et al., Nucl. Phys. A 706 (2002) 203.
[14] A. Formicola, et al., Phys. Lett. B 591 (2004) 61.
[15] A. Lemut, et al., Phys. Lett. B 634 (2006) 483.
[16] A. Formicola, et al., Nucl. Instrum. Methods Phys. Rev. A 507 (2003) 609.
[17] Gy. Gyürky, et al., Phys. Rev. C 75 (2007) 35805.
[18] F. Confortola, Astrophysical $S$-factor of the $^3$He$(\alpha, \gamma)^7$Be reaction measured at low energy by prompt and delayed $\gamma$ detection, PhD Thesis in Physics, Università degli Studi di Genova, February 2007.
[19] J. Görres, et al., Nucl. Instrum. Methods Phys. Rev. 177 (1980) 295.
[20] M. Marta, et al., Nucl. Instrum. Methods Phys. Rev. A 569 (2006) 729.
[21] A. Caciolli, et al., Eur. Phys. J. A, submitted for publication.
[22] T.A. Tombrello, P.D. Parker, Phys. Rev. A 131 (1963) 2582.
[23] C. Arpesella, et al., Nucl. Instrum. Methods Phys. Rev. A 360 (1995) 607.
[24] H. Kräwinkel, et al., Z. Phys. A 304 (1982) 307.
[25] B.T. Kim, T. Izumoto, K. Nagatani, Phys. Rev. C 23 (1981) 33.
[26] P. Parker, R. Kavanagh, Phys. Rev. 131 (1963) 2578.
[27] K. Nagatani, M.R. Dwarakanath, D. Ashery, Nucl. Phys. A 128 (1969) 325.
[28] J. Osborne, et al., Phys. Rev. Lett. 48 (1982) 1664.
[29] Q.K.K. Liu, et al., Phys. Rev. C 23 (1981) 645.
[30] T. Kajino, Nucl. Phys. A 460 (1986) 559.
[31] P. Descouvemont, et al., At. Data Nucl. Data Tables, Sect. A 88 (2004) 203.
[32] T. Kajino, H. Toki, S.M. Austin, Astrophys. J. 319 (1987) 531.
[33] C. Rolfs, W.S. Rodney, Cauldrons in the Cosmos, University of Chicago Press, 1980.
[34] A. Lemut, Eur. Phys. J. A 36 (2008) 233.
[35] J. Ziegler, SRIM 2003.26, http://www.srim.org.
[36] D. Bemmerer, et al., Phys. Rev. Lett. 97 (2006) 122502.
[37] F. Confortola, et al., Phys. Rev. C 75 (2007) 065803.

[38] T.A.D. Brown, et al., Phys. Rev. C 76 (2007) 055801.
[39] R.G.H. Robertson, P. Dyer, T.J. Bowles, R.E. Brown, N. Jarmie, C.J. Maggiore, S.M. Austin, Phys. Rev. C 27 (1983) 11.
[40] H. Volk, et al., Z. Phys. A 310 (1983) 91.
[41] T. Alexander, et al., Nucl. Phys. A 427 (1984) 526.
[42] M. Hilgemeier, et al., Z. Phys. A 329 (1988) 243.
[43] A. Cśotó, K. Langanke, Few-Body Syst. 29 (2000) 121.
[44] Particle Data Group, J. Phys. G 33 (2006) 1.
[45] F. Strieder, C. Rolfs, Prog. Part. Nucl. Phys. 59 (2007) 562.
[46] W.C. Haxton, A.M. Serenelli, arXiv: 0805.2013 [astro-ph].
[47] M.C. Chen, Am. Inst. Phys. Conf. Ser. 944 (2007) 25.
[48] M. Asplund, et al., Astron. Soc. Pacific Conf. Ser. 336 (2005) 25.